

# Sensitivity enhancement of an integrated micro-fluidic system, based on diffraction under total internal reflection\*

Y. SAROV<sup>a,b\*</sup>, TZ. IVANOV<sup>a</sup>, V. SAROVA<sup>c</sup>, I. CAPEK<sup>d</sup>, I. W. RANGELOW<sup>a</sup>

<sup>a</sup> *MNES, IMNE, FEI, Technical University of Ilmenau, PF 100565, 98684 Ilmenau, Germany*

<sup>b</sup> *Central Laboratory of Optical Storage and Processing of Information, Bulgarian Academy of Sciences, P.O. Box 95, 1113 Sofia, Bulgaria*

<sup>c</sup> *Institute of Electronics, Bulgarian Academy of Sciences, 72 Tzarigradsko Chaussee, 1784 Sofia, Bulgaria*

<sup>d</sup> *Polymer Institute, Slovak Academy of Sciences, 9 Dubravská cesta, 842 36 Bratislava, Slovakia*

This work reports an enhancement of the diffraction efficiency of a grating upon total internal reflection, which is the main part in a recently developed integrated system for micro-fluidic analysis. Experimentally, a first order diffraction efficiency of 37% is obtained, by adjusting the thickness and/or the refractive index of a thin transparent layer, which seals and isolates the grid. The application of such an optimized grating to micro-fluidic sensing increases the accuracy of the whole system by a factor of two.

(Received November 5, 2008; accepted December 15, 2008)

*Keywords:* Sensors; Micro-fabrication; Total internal reflection; Diffraction gratings

## 1. Introduction

The convergence of microfabrication technologies, novel materials and techniques for medical, biochemical and microbiological analysis enables the realisation of so-called micro-total analysis systems ( $\mu$ -TAS) [1]. They benefit from fast, low-cost, automated chemical analysis using minimal samples in a multiplicity of applications [2,3]. The advance of  $\mu$ -TAS motivates the further development of compatible methods for micro-fluidic sensing [4].

Recently, an integrated optical micro-fluidic system for the recognition, investigation and analysis of pico-liters of mixtures [5] or nano-disperse fluidic samples [6] has been demonstrated. The system employs an integrated diffraction grating, sealed by an isolating layer of SiN<sub>x</sub> and illuminated under total internal reflection (TIR). The light diffracted from the grid is sensitive to the fluidic optical constants due to the evanescent TIR field, which penetrates into and interacts with the investigated micro-fluids [7,8].

The 1<sup>st</sup> order diffraction efficiency (DE)  $\eta$ , used as a sensing signal, depends directly on the properties of the sealing layer, since the light crosses the SiN<sub>x</sub> film twice.

The aim of this work is to produce highly sensitive micro-fluidic systems by adjusting the thickness and/or the refractive index (RI) of the sealing layer. The sensors exhibit a maximum  $\eta$  when the optical path in the sealing layer matches the interference enhancement condition. A two times higher higher analyte resolution is achieved in such a case, as compared to the sensitivity of analogous fluidic systems without optimization of the diffraction, as reported in [5].

## 2. Theory and experiment

A schematic representation of the micro-fluidic sensor is shown in Fig. 1. The diffraction grating defines periodical changes of the reflection. The amplitude of the light totally reflected from the lines spacing  $r$ , depends on the fluidic absorption, while its phase  $\Phi$  changes with the fluidic refractive index [8]. The TIR light interferes with the reference light from the metal lines, which is considered constant. The energy distribution between the resulting diffraction orders depends on both fluidic optical constants.

\* Paper presented at the International School on Condensed Matter Physics, Varna, Bulgaria, September 2008

An analytical description of TIR diffraction is offered by the model of the amplitude transmission [9]. The 1<sup>st</sup> order DE  $\eta$  in this case is given by:

$$\eta = \frac{1}{\pi^2} [r_t^2 + r_m^2 - 2r_t r_m \cos(\Phi_t + \Phi_d - \Phi_m)] \quad (1)$$

where  $r_m$  and  $\Phi_m$  are the amplitude and the phase of the light reflected from the metal lines. The additional phase shift  $\Phi_d$  is related to the light propagation within the space of the diffraction grating and in the sealing layer:

$$\Phi_d = \frac{4\pi}{\lambda} \left( \frac{d_n n_d}{\sqrt{n_d^2 - n_p^2 \sin^2 \varphi}} + \frac{d_g n_1}{\cos \varphi} \right) \quad (2)$$

where  $d_n$  and  $n_d$  are the thickness and the RI of the sealing layer and  $d_g$  is the thickness of the grating. It should be noted that the metallic and the TIR amplitudes and phases are polarization dependent, as in the exact equations given e.g. in [8].

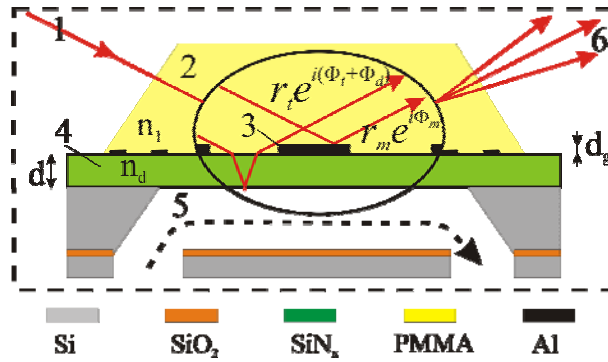


Fig. 1. Cross-sectional view of the micro-fluidic sensor: 1- incident laser beam, 2- PMMA TIR prism, 3- diffraction grating, 4- SiNx sealing layer, 5- micro-channel, 6- diffraction pattern.

The integrated sensor is fabricated by fitting together three Si <100> wafers - w1, w2 and w3. The cavities, corresponding to the inverted prisms (2) are micro-fabricated in w1 by anisotropic potassium hydroxide (KOH) etching. A zero-stress SiNx sealing layer (4) is deposited on the top of w2. Subsequently, an Al grid (3) is realized by a lift-off technique. The SiO2 on the bottom of w2 is patterned to create a mask for the micro-fluidic channel (5). The wafer w1 is filled with molten polymethylmethacrylate (PMMA) and pressed onto the grating side of w2, hot embossing the prisms. As a next step, the bonded wafers w1 and w2 are etched in KOH until the SiNx membrane is exposed. Thus, the micro-channel (5) and the PMMA prism (2) are simultaneously released. The in- and out-lets are wet etched in w3, which is finally bonded to w2 to cover the micro-channel.

The fabrication of the sealing SiNx layer is a key step, feasible for the optimization of  $\eta$ . Different SiNx layers are realized by plasma enhanced chemical vapor deposition (PECVD) in an Oxford Plasma 80 system at 650 mTorr chamber pressure. Cycled deposition at high and low RF frequency is used for deposition of zero-stress SiNx films [10]. The sealing layers differ in the thickness  $d$  and/or the composition  $x$ . The first parameter is controlled by the deposition time, and the second by the gas flows and the deposition temperature  $T$ . These parameters of the fabricated SiNx layers, together with the deposition conditions are given in Table 1. The films' refractive index at  $\lambda=633\text{nm}$  has been measured by an ellipsometer at  $70^\circ$  and is also shown in Table 1. Each SiNx film has been further used for fabrication of a complete micro-fluidic sensors.

Table 1. PECVD conditions, thickness and refractive index of the SiNx layers.

No.	SiH <sub>4</sub> /NH <sub>3</sub> /N <sub>2</sub> flow [sccm]	T deposit. [°C]	d [nm]	refract. index.
1	20/20/980	350	100	1.952
2	20/20/980	350	200	1.952
3	20/20/980	350	300	1.952
4	20/20/980	350	400	1.952
5	10/20/990	120	350	1.818
6	15/20/985	250	350	1.891
7	20/20/980	350	350	1.952
8	30/5/970	400	350	2.045

The setup for measurements can be discussed with the help of Fig. 1. A linear polarized diode laser ( $\lambda=635\text{ nm}$ ) is used as a light source (1). The beam is directed to the prism facet, fulfilling the TIR condition for the interface between the micro-prism (2) and the fluid in the micro-channel (5). The Al grating (3) with thickness  $d_g=60\text{nm}$  and a period  $\Lambda=10\mu\text{m}$  causes a diffraction pattern in reflection (6). The measurements are taken both for s and p polarization of the light, which is adjusted by a rotator of the polarization. In all our experiments, the angle of the incident beam exceeds the critical angle by  $1^\circ$ . The changes in the optical constants of the fluid can be determined by measuring the 1<sup>st</sup> order DE [5,8]. It is realized by fixed photodetector, since the angles for the diffraction patterns are constant [7, 8].

## 2. Results and discussion

Equations (1) and (2) give the dependence of the 1<sup>st</sup> order DE  $\eta$  on the thickness  $d$  and the RI  $n_d$  of the sealing SiNx layer. The theory is illustrated in Figs. 2a and 2b, for

the case of transverse electric (s) and transverse magnetic (p) light polarization, respectively. The theoretical simulations are made for the exact geometry and composition of the described micro-system and for the case of water-based solution sensing (i.e. samples with RI close to that of water). Actually, the calculation of the theoretical 3D profiles in Fig. 2 have given the beneficial  $\text{SiN}_x$  thicknesses and RI, which were later realized (Table 1).

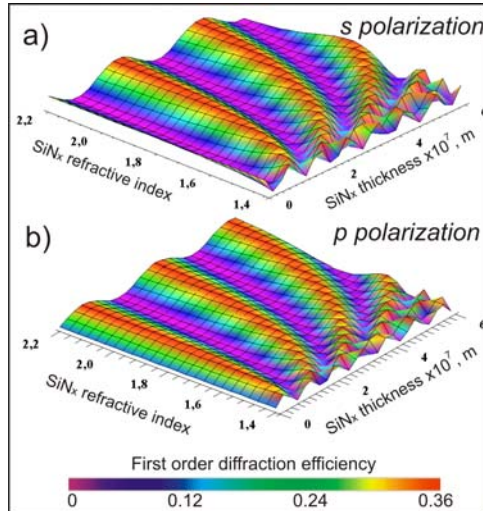


Fig. 2. Dependence of  $\eta$  on the  $\text{SiN}_x$  thickness and RI for a)- s polarized and b)- p polarized light.

Fig. 3 shows a picture of fabricated micro-sensor, placed in a special holder, which ensures the fluidic supply. A comparison with a coin of 1 eurocent gives an impression of the dimensions of the whole system.

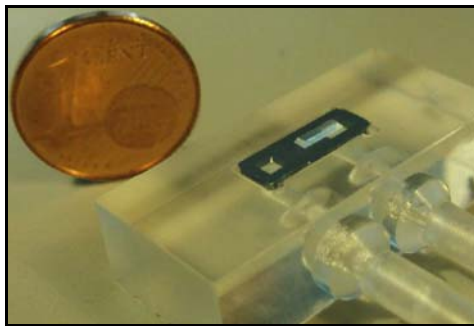


Fig. 3. View of the integrated micro-fluidic system.

The obtained results of the 1<sup>st</sup> order DE for sensors with different thickness of the sealing layer for the both orthogonal polarizations are presented in Fig. 4. The theoretical error, shown as an error bar is estimated as 15%. At the same time, the reproducibility error is below 5%, as calculated by statistical processing of the data taken in repeated measurements. The theoretical curves are also presented in the figure. They are periodic functions of  $d$ , as shown by Eq. (1-2). It can be seen that the behavior of  $\eta$  is

opposite for s and p polarizations. The maxima of the 1<sup>st</sup> order DE for s polarization correspond to minima for p polarization and vice versa. The reason is in the different TIR phases at s and p polarization. Hence, an enhancement of  $\eta$  for any polarization is not possible.

The sensor, sealed by layer No. 2 exhibits the highest 1<sup>st</sup> order DE of 37% for s polarization, while the sensor with layer No. 3 has  $\eta = 34\%$  for p polarization. These values are close to the theoretical maximum  $\eta_{\max} = (r_t + r_m)^2 / \pi^2 \approx 38\%$ . It is achieved, when the cosine term in equation (1) is equal to -1, i.e. the additional phase shift  $\Phi_d$  in the sealing layer matches the condition for constructive interference.

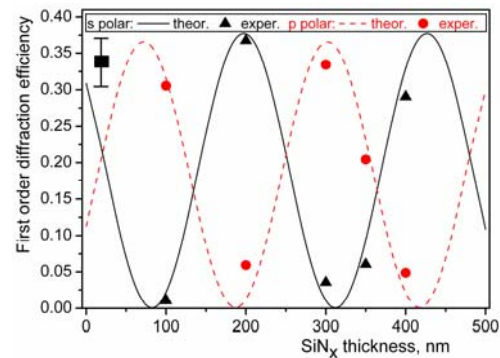


Fig. 4. Dependence of efficiency  $\eta$  on the  $\text{SiN}_x$  thickness-theory vs. experiment.

Fig. 5 presents the dependence of  $\eta$  on the RI of the  $\text{SiN}_x$  layer. The measurements for s and for p polarization are compared with the theoretical curves. Again, the measurements' data from Fig. 5 agree with the theory, within the accuracy of 15%.

The results in Fig. 5 prove that the  $\text{SiN}_x$  RI has a significant influence on the diffracted energy distribution. Even a RI variation of about 12% results in an almost complete change of  $\eta$  between the two extremes. Here the orthogonal polarizations also have opposite influences on the 1<sup>st</sup> order diffraction efficiency as a function of the RI.

The variation of the thickness and RI of the sealing layer have analogous effects only at normal incidence, which is in contradiction with the TIR condition. It is clear that  $\eta$  can be optimized either by setting the appropriate thickness or RI of the sealing layer. However, the possibility to opt between these two parameters gives more flexibility of the fabrication technology. Also, an appropriate combination of  $d$  and  $n_d$  at a fixed angle of incidence can be used to reduce the particular waveguided propagation of the light into the sealing layer and into the micro-channel. Such an effect is considered as parasitic, because it results in multiple diffraction patterns, which are spatially shifted from the fundamental one.

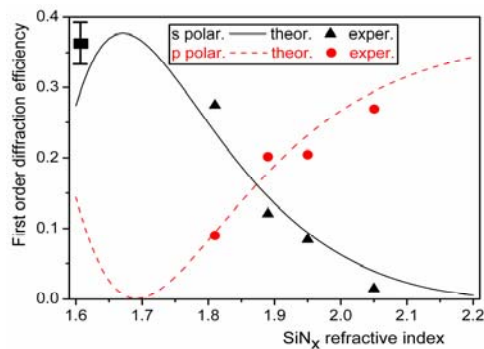


Fig. 5. Dependence of the efficiency  $\eta$  on the  $\text{SiN}_x$  refractive index- theory vs. experiment.

The dependence of the sensing accuracy on  $\eta$  is investigated in Fig. 6. Measurements of methylene blue solutions, as described in [5], are here repeated with the sensors with layers 2 and 3, optimized for s and p polarization respectively. In all cases, the DE  $\eta = \eta_0 + k.c$  decreases linearly with the concentration of the analyte  $c$ , where  $\eta_0$  is the DE for the solvent ( $\text{H}_2\text{O}$ ). The concentration resolution  $\Delta c$  is defined as  $\Delta c = \Delta\eta/k$ , where  $\Delta\eta$  is the DE error, determined by repeated measurements and calibration. Thus, the sensors 2 and 3 with enhanced  $\eta$  show approximately twice the sensitivity of the sensor from [5] without optimized diffraction.

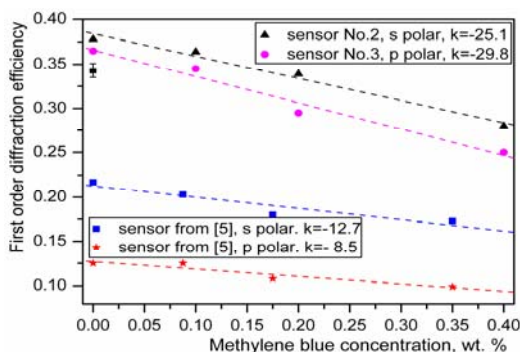


Fig. 6. Comparison between the sensors with layers 2 and 3 with that from [5].

Three facts determine a diffraction order with enhanced DE as sensitivity-beneficial. Firstly, the concentration response  $k$  is higher, i.e.  $\Delta c$  is smaller for a stronger order. Secondly, the detection of stronger signals by a detector with fixed accuracy is more exact. Finally, under given experimental conditions the measurements of

orders of different strengths have a similar error  $\Delta\eta$  (shown as a bar in Fig. 6). This could be explained by the contribution of an error of about 2% of the incident power, independent of the detection accuracy and the optical adjustment. It is probably related to the background illumination due to the multiple diffraction patterns, fluctuations of the laser power, multiple reflections, etc.

### 3. Conclusions

This work reports the enhancement of the first order diffraction efficiency of a grating order under total internal reflection. For this purpose,  $\text{SiN}_x$  layers with different thickness (100-400nm) and 12% variation of the refractive index are realized. Experimentally, the maximum first order diffraction efficiency of 38% is achieved. The sealing  $\text{SiN}_x$  films are applied for realization of integrated systems for micro-fluidic analysis, and a doubled increase in the sensitivity is reported.

### Acknowledgements

This work is supported by the Alexander von Humboldt Foundation.

### References

- [1] H. Hunt, J. Wilkinson, *Microfluid. Nanofluid.* **4**, 53 (2008).
- [2] A. deMello, *Nature* **442**, 394 (2006).
- [3] S. Lee, S. Lee, *Appl. Microbiol Biotechnol.* **64**, 289 (2004).
- [4] J. Wang, G. Chen, A. Muck, J. Collins, *Electrophoresis* **24** 3728, (2003).
- [5] Y. Sarov, T. Ivanov, V. Sarova, I. Capek, I. Rangelow, *Appl. Phys. A* **84**, 191 (2006).
- [6] Y. Sarov, I. Capek, T. Ivanov, V. Sarova, I. Rangelow, *NanoLett.* **8**, 375 (2008).
- [7] S. Sainov, *Sens. Actuat. A* **45**, 1 (1994).
- [8] Y. Sarov, S. Sainov, *J. Opt. A: Pure Appl. Opt.* **4**, 382 (2002).
- [9] V. Ovchinnikov, Yu. Udov, *Opt. Spectr.* **45**, 202 (1978).
- [10] F. Habraken, A. Kuiper, *Mat. Sci. Eng.* **R12**, 123 (1994).

\* Corresponding author: ysarov@yahoo.com